Circular Hollow Section X-Connections near an Open Chord End: Stress Concentration Factors

by

Ali Ziaei Nejad, Min Sun*
Department of Civil Engineering, University of Victoria, Victoria, British Columbia V8P 5C2, Canada
and

Kyle Tousignant
Department of Civil & Resource Engineering, Dalhousie University, Halifax, NS, B3H 4R2, Canada

Abstract

This paper presents a numerical finite element (FE) investigation to determine stress concentration factors (SCFs) for circular hollow section (CHS)-to-CHS X-connections near an open chord end. Previous large-scale experiments are used to validate FE models, and a parametric study is performed. The parametric study consists of 240 models with variations in chord slenderness (2*γ*), branch-to-chord diameter ratio (*β*), branch-to-chord thickness ratio (*τ*), and chord end distance (*e*) on one side of the of the connection. For each of the 240 models, SCFs are determined at the crown and saddle hot-spot stress locations. Extrapolating existing formulae to predict "end-distance effects" on SCFs at these locations in CHS-to-CHS X-connections, from CIDECT Design Guide 8 (DG8), is shown to be inaccurate. Hence, SCF correction coefficients (*ψ*) and parametric formulae to estimate *ψ* (based on e/d_0, 2*γ* and *β*) are derived.

Key words

Circular hollow sections; X-connections; end-distance effects; stress concentration factors; fatigue design; cap plates.

*Corresponding Author. E-mail: msun@uvic.ca

1. Introduction

Design procedures for hollow structural section (HSS) connections under static and fatigue loading have been developed and implemented in several design standards and guidelines internationally [1-10]. These standards and guidelines in general contain prescriptive design tables for classic failure modes (or limit states) and connection types (e.g. T-, X- and Y-connections) that are commonly specified in construction.

This prescriptive approach has two advantages:

(1) It provides a physical understanding of the limit states that need to be checked. More importantly, it allows users of design tables to understand HSS connection behaviour and – when necessary – to extrapolate this behaviour and use “engineering judgment” to design other connection types that are beyond the scope of the tables; and

(2) For designers familiar with a given process and standard (e.g. [7,9]), it is relatively fast and easy to apply without having to perform significant job-specific calculations.

The design rules in [1-10] have, in general, been premised upon having an HSS chord member that is sufficiently long on both sides of the connection, to avoid having to explicitly consider the effects of chord length and chord end boundary conditions on connection behaviour [11,12]. These effects are herein called “chord end-distance effects”. Put simply, these rules are premised upon having a large end distance (*e*, in Fig. 1a) on both sides of the connection.

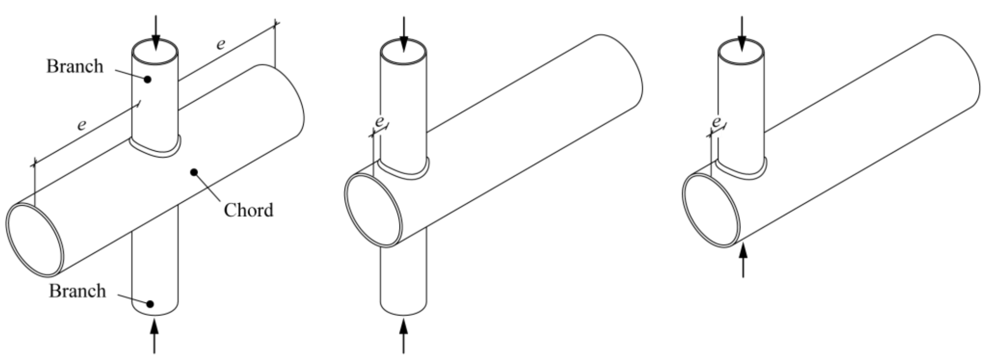

(a) (b) (c)

Fig. 1. CHS-to-CHS X-connections: (a) regular connection; (b) and (c) end connections

Definitive guidance on the design of HSS connections with branch(es) near a chord end (or "end connections", as shown in Figs. 1b,c) is limited. Hence, designers generally resort to strengthening such connections via cap plates (or end plates), doubler plates, or diaphragms [12]. This can be an expensive and unnecessary practice.

To address this issue, new limits of applicability have recently been added to design equations in Chapter K of AISC 360 [7] for plate-to-HSS and HSS-to-HSS connections under static loading. These limits provide the minimum end distance (e_{min}) "from the near side of the connecting branch or plate to the chord end" required to develop the static strength of the connections predicted by the AISC 360-16 Chapter K equations [7]. Similar e_{min} limits are provided in prEN1993-1-8 Clause 9.1.2(10) for HSS-to-HSS connections [13]. The underlying (and subsequent) research on the topic of end-distance effects on the static strength of HSS-to-HSS connections is well-documented in [11,12,14-18].

For CHS-to-CHS connections under static loading, the current e_{min} values in AISC 360-16 Chapter K [7] are generally conservative for ensuring that the full strength of the connection and weld (based on corresponding design equations) can be developed [11,12,18]. However, there has been little research on the influence of chord end-distance effects on the fatigue life of CHS-to-CHS connections [19]. This paper hence presents a study on stress concentration factors (SCFs) for CHS-to-CHS X-connections situated near an open chord end (Fig. 1b), which frequently occur at the end of CHS trusses or girders.

The scope of the work covered in this paper includes: (a) a review of recent research on HSS end connections; (b) a summary of large-scale experiments used to validate finite element (FE) models for determination of SCFs; (c) a parametric study consisting of 240 FE models with varied chord slenderness ($2\gamma = d_0/t_0$, where d_0 = chord diameter and t_0 = chord thickness), branch-to-chord with ratio ($\beta = d_1/d_0$, where d_1 = branch diameter), branch-to-chord thickness ratio ($\tau = t_1/t_0$, where t_1 = branch thickness) and e (on one side of the of the connection) (see Fig. 2); (d) an evaluation of the existing SCF formulae given in CIDECT Design Guide 8 (DG8) [5] applied to the CHS-to-CHS end connections covered herein; and (e) calibration of parametric formulae to estimate SCF correction coefficients (ψ) based on non-dimensional parameters (e/d_0, 2γ and β).

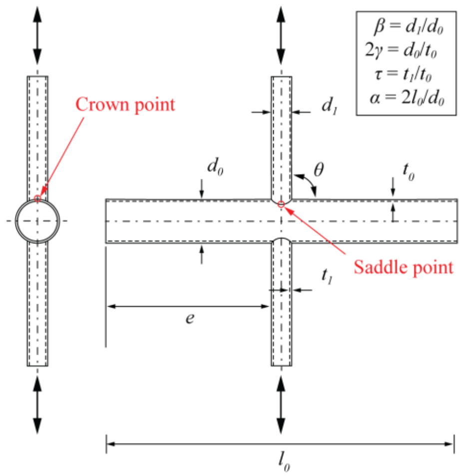

Fig. 2. CHS-to-CHS X-connection terminology *(one-column figure)*

2. Recent research on HSS end connections

Recent research on HSS end connections [11,12,14-18] has shown that their static structural behaviour can differ considerably from so-called “regular connections”. For RHS-to-RHS X-connections, this was illustrated by Fan & Packer [11], for chord plastification limit state. While existing design formulae assume sufficient e on either side of a connection to development a characteristic yield-line mechanism (see Fig. 3 of [11]) , Fan & Packer [11] showed that, for end connections, a modified yield-line patterns develops. This results in a lower static strength when compared to regular connections (with all else being equal) when the ends are left open. Bu & Packer [12] extended this research to cover sidewall buckling of RHS-to-RHS X-connections. For branch plate- and CHS-to-CHS T- and X-connections, Van der Vegte & Makino [16,17] demonstrated a similar phenomenon, showing a reduction in the static strength of end connections with open chord ends. Tousignant [18] showed that this result extends to welds in CHS-to-CHS X-connections when designed as fit-for-purpose.

To address these phenomena, the following e_{min} values appear in the “Limits of Applicability” for branch plate- and HSS-to-HSS connection design equations in AISC 360-16 [7]:

- For branch plate-to-CHS connections under axial load (Table K2.1A):

$$e_{\min} = d_0\left(1.25 - \frac{b_p / d_0}{2}\right) \quad (1)$$

- For CHS-to-CHS T-, Y-, X- and K-connections (Table K3.1A):

$$e_{\min} = d_0\left(1.25 - \frac{d_1 / d_0}{2}\right) \quad (2)$$

- For RHS-to-RHS T- and Y-connections (Table K3.2A):

$$e_{\min} = b_0\sqrt{1 - b_1 / b_0} \quad (3)$$

where b_p = branch plate width; b_1 = branch width; and b_0 = chord width.

Eqs. (1) and (2) are based on old rules for the design of offshore tubular structures; they are knowingly conservative (see [16,17]) and are intended to cover many types of connections and loadings.

When $e < e_{min}$, the AISC 360-16 [7] Chapter K Commentary suggests that the strengths predicted by using HSS connections design formulae in Tables K3.1 and K3.2 can conservatively be reduced by 50% if connection reinforcement (e.g. a chord end/cap plate) is not provided. Bu & Packer [12] have since shown that even a 40% reduction is conservative in that case.

As noted in Section 1, EN 1993-1-8 [9], via prEN1993-1-8 Clause 9.1.2(10) [13], also includes a minimum end distance(s) – like AISC 360-16 Chapter K [7]; however, a clear disparity can be found by comparing the e_{min} values between these two codes. Detailed discussions on prEN1993-1-8 Clause 9.1.2(10) [13] can be found in [19], where the following two limitations related to it are noted:

(1) prEN1993-1-8 Clause 9.1.2(10) [13] was developed primarily based on numerical (FE) research by van der Vegte and Makino [16] on isolated CHS-to-CHS connections that were symmetric about the branch centerline. Hence, its applicability to "end connections" that are not symmetric about the branch centerline (e.g. Fig. 1b) is unknown.

(2) In prEN1993-1-8 Clause 9.1.2(10) [13], the requirement for CHS connections is transcribed to cover RHS connections. This has been done by replacing the CHS external diameter (d_0) with the RHS external width (b_0). No research evidence was available at the time to support this transcription.

It should also be appreciated that the above minimum end distance (e_{min}) values, in both AISC 360-16 and prEN1993-1-8, cater to end connections under static loading. Research on the chord end-distance effects on fatigue loading [via its influence on stress concentration factors (SCFs)] is still rather limited.

2.1 Research on SCFs in HSS end connections

Early research by Efthymiou and Durkin [20] showed that SCFs at the chord and branch saddle locations of CHS-to-CHS connections decrease as the chord length decreases. However, this research included: (a) only connections symmetrical about the branch(es) [see (1), above]; and (b) end distances (*e* in Fig. 2) that were, in general, larger than practical values for end connections. This research forms the basis of the "F_2 factor" used in the CIDECT DG8 [5] (see Section 3).

More recently, Daneshvar et al. [19] performed an FE parametric study to determine SCFs in directly welded RHS-to-RHS axially loaded X-connections near an open chord end. SCFs were determined at the critical hot spots in both regular and end connections [with varying e/b_0, β (= b_1/b_0, for RHS) and 2γ (= b_0/t_0) ratios]. For the end connections, existing formulae in CIDECT DG8 to predict SCFs in regular RHS-to-RHS X-connections were shown to be conservative, and a parametric formula to estimate the SCF correction coefficient(s) ψ (based on $e/b0$, 2γ and β) was developed. The following seeks to address the same design issue for CHS-to-CHS X-connections under fatigue loading.

3. SCF formulae in CIDECT DG8

The fatigue life of HSS connections is commonly correlated to localized hot spot stresses at various locations around the joint. Using hot spot stresses and fatigue strength curves (S-N curves), the permissible number of load cycles of connections can be determined. For most tubular structures, the hot-spot stress provisions of CIDECT DG8 [5], which use symbol definitions consistent with Fig. 2, are widely used internationally. For determination of the fatigue life of a CHS-to-CHS X-connection under branch axial loading, CIDECT DG8 prescribes the calculation of hot spot stresses at critical locations that include crown and saddle points (see Fig. 2) on the branch and chord member. Hot spot stresses are the product of the branch nominal stress × an SCF, where SCF formulae are given in [5]. These formulae are reproduced below [Eqs. (4) – (13)].

As shown: (1) they are functions of non-dimensional parameters (i.e. β, τ, γ and α); and (2) they acknowledge the chord end-distance effect through the parameter F_2.

- For the chord:

$$SCF_{ch\_saddle,ax} = X_1 \cdot F_2 \tag{4}$$

$$SCF_{ch\_crown,ax} = X_2 \tag{5}$$

where $SCF_{,ch\_saddle,ax}$ = chord SCF at the saddle point; $SCF_{ch\_crown,ax}$ = chord SCF at the crown point; and F_2 = correction factor for the chord end-distance effect.

- For the branch(es):

$$SCF_{b\_saddle,ax} = X_3 \cdot F_2 \tag{6}$$

$$SCF_{b\_crown,ax} = X_4 \tag{7}$$

where $SCF_{,b\_saddle,ax}$ = branch SCF at the saddle point; and $SCF_{b\_crown,ax}$ = branch SCF at the crown point.

The parameters X_1, X_2, X_3, X_4 and F_2 are given in CIDECT DG8 [5] as:

$$X_1 = 3.87 \cdot \gamma \cdot \tau \cdot \beta \left[1.10 - \beta^{1.8}\right] \cdot \left(\sin\theta\right)^{1.7} \tag{8}$$

$$X_2 = \gamma^{0.2} \cdot \tau \left[2.65 + 5 \cdot \left(\beta - 0.65\right)^2\right] - 3 \cdot \tau \cdot \beta \cdot \sin\theta \tag{9}$$

$$X_3 = 1 + 1.9 \cdot \gamma \cdot \tau^{0.5} \cdot \beta^{0.9} \cdot \left(1.09 - \beta^{1.7}\right) \cdot \sin^{2.5}\theta \tag{10}$$

$$X_4 = 3 + \gamma^{1.2} \cdot \left[0.12 \cdot \exp\left(-4 \cdot \beta\right) + 0.011 \cdot \beta^2 - 0.045\right] \tag{11}$$

If $\alpha \geq 12$: $$F_2 = 1.0 \tag{12}$$

If $4 \leq \alpha < 12$: $$F_2 = 1 - \left(1.43 \cdot \beta - 0.97 \cdot \beta^2 - 0.03\right) \cdot \gamma^{0.04} \cdot \exp\left(-0.71 \cdot \gamma^{-1.38} \cdot \alpha^{2.5}\right) \tag{13}$$

where θ = acute angle between the branch and chord (in degrees) and α = chord length parameter (= $2l_0/d_0$, where l_0 = chord length) (see Fig. 2).

Eqs. (4)-(13) are valid within the ranges $0.2 \leq \beta \leq 1.0$, $15 \leq 2\gamma \leq 64$, $0.2 \leq \tau \leq 1.0$, $4 \leq \alpha \leq 40$, and $30° \leq \theta \leq 90°$, and CIDECT DG8 [5] also recommends a minimum SCF of 2.0 for all locations.

By plotting F_2 versus different values of α (Fig. 3a,b), it can be see that F_2 can become quite small within the range of validity of the formula (i.e. $4 \leq \alpha \leq 40$), indicating that the chord end-distance effect on SCFs is large (but, in this case, beneficial) for CHS-to-CHS X-connections. Presumably, these equations apply to connections with open chord ends; however:

(1) when $\alpha < 12$, the CIDECT DG8 formulae only cover CHS-to-CHS connections that are symmetric about the branch centerline (like the e_{min} values in prEN1993-1-8 Clause 9.1.2(10) [13]); and

(2) for practical "end connections", e/d_0 ranges from about 0.1 to 1.0 [11,12,18], which can be shown to be smaller than the lower bound of $\alpha = 4$ in Eq. (13).

Figs. 3a,b also show an extrapolation of Eq. (13) for $\alpha < 4$, to illustrate the potential influence of chord end-distance effects on CHS-to-CHS X-connections covered by this range. Although rational, at present, there is no research evidence available to support this extrapolation.

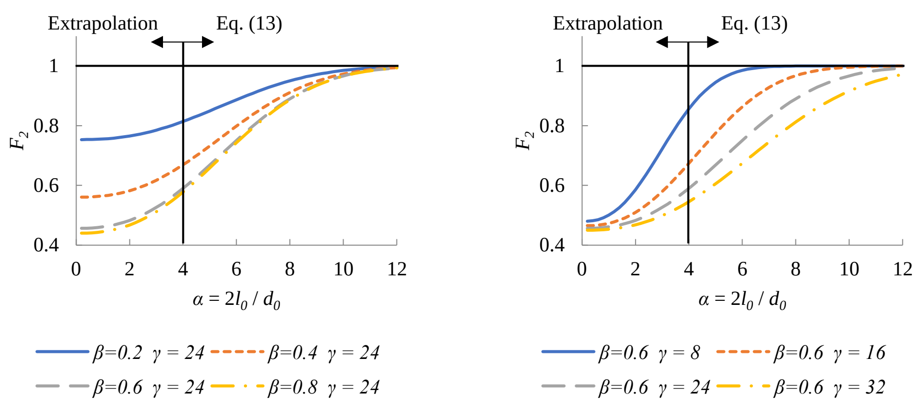

(a) Effect of β (γ = 24) (b) Effect of γ (β = 0.6)

Fig. 3. Effects of chord length and non-dimensional parameters on SCFs in CHS-to-CHS axially loaded X-connections based on CIDECT DG8 [5] and extrapolation

4. Summary of experimental data

In this research, experimental data from testing of steel CHS-to-CHS X-connections connections in the Offshore Technology Report prepared by Lloyd's Register of Shipping for the Health and Safety Executive (HSE) in the UK [21] is used for validation of FE modelling. The measured SCFs at the four hot spot locations (chord saddle, chord crown, branch saddle and branch crown) for four connections from the report (with varying τ, β, 2γ and α) are summarized in Table 1.

Table 1. Summary of SCFs from CHS-to-CHS X-connection tests [21]

			Non-dimensional parameters [(2)]				Experimental SCFs			
Connection No.	d_0 (mm)	θ	τ	β	γ	α	Chord saddle	Chord crown	Branch saddle	Branch crown
1	473	90°	0.94	0.72	10.4	8.5	10.9	- [(1)]	7.5	-
2	684	90°	0.56	0.50	8.6	5.8	4.8	-	4.5	-
3	508	90°	0.79	0.38	20.7	9.8	21.8	3.3	10.6	1.5
4	407	90°	0.82	0.67	25.3	17.5	29.5	-	15.0	-

[(1)] Experimental data was unavailable at this location.
[(2)] See Fig. 2 for non-dimensional parameter definitions.

5. Preliminary finite element analysis

5.1 Connection modelling

Four FE models were created in ANSYS [22] using the measured dimensions of the connection specimens in Table 1. The modelling approach used by [18,23-26] was adopted in this research, which is consistent with the recommendations given in CIDECT DG8 [5]. As shown in Fig. 4 (on the following page), four layers of eight-noded solid elements (SOLID45 in ANSYS) through the branch and chord wall thicknesses were used.

A literature survey was performed on previous research that involved modelling of welds in hollow section connections [27-39]. The weld modelling approaches therein were found to be consistent. Therefore, in Section 5 a similar approach was adopted, and the weld was modelled by using the profile and dimensions shown in Fig. 4. The weld leg sizes on the branch side and the chord side are $1.0t_1$ and $0.5t_1$, respectively. The same weld shape and dimensions are applied in the FE parametric study in Section 6.

Linear elastic properties [i.e. Young's modulus (E) = 200 GPa, and Poisson's ratio (v) = 0.3] were applied to both the steel and weld materials in the FE models. Considering the symmetry of geometry, loading and boundary conditions, only one half of each of the four connection specimens was modelled with symmetry boundary conditions applied along the "cut" face (see Fig. 4). (Note that one eighth of each connection could instead have been modelled, due to symmetry about a second plane).

The connection models contained fixed nodes at the bottom end of the lower branch, while the nodes on the top end of the top branch were free. The chord ends were pin-supported. (Since the aim of the research is to develop modifications to the existing formulae in CIDECT DG8 [5], the applied boundary conditions are consistent with those recommended in the guideline for CHS-to-CHS connections with “general chord fixity conditions”. The applied boundary conditions also simulate typical experimental/numerical research setups [20]).

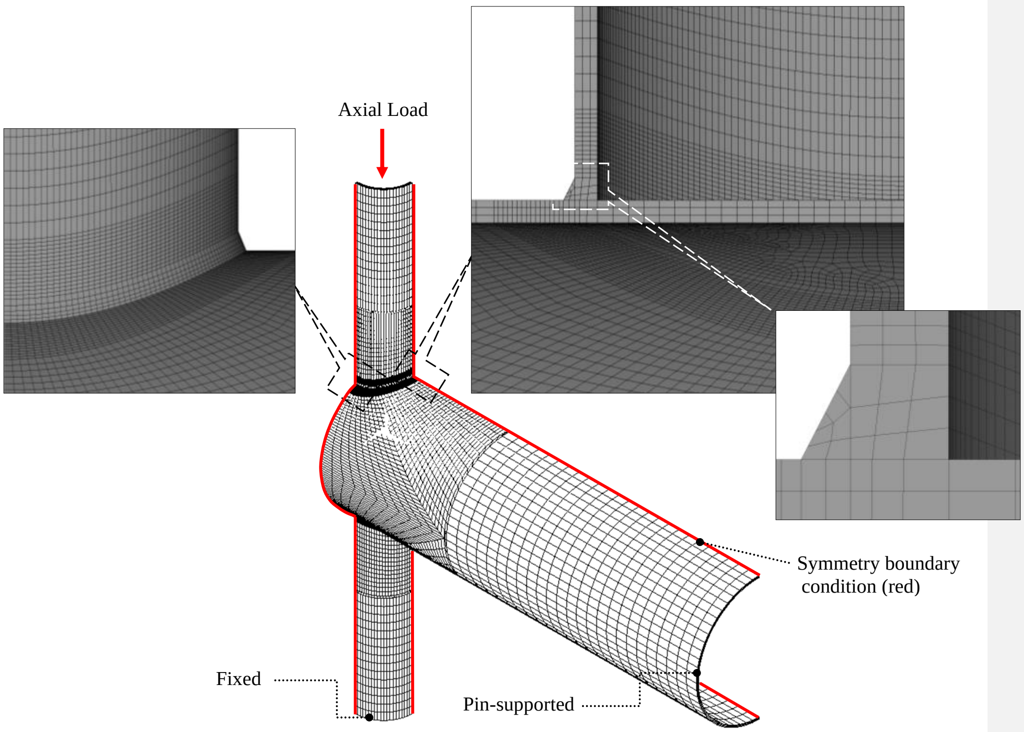

Fig. 4. Typical CHS-to-CHS X-connection FE model *(two-column figure)*

As shown in Fig. 5, the welded joint location was carefully partitioned (Fig. 5a) and finely meshed (Fig. 5b) (following the recommendations in CIDECT DG 8 [5] and suggestions from previous research [18,23-39]). The aim of this was to allow accurate determination of stresses perpendicular to the weld toe within the "extrapolation region(s)" recommended by DG8 [5], as shown in Fig. 6. The definitions for $L_{r,min}$ and $L_{r,max}$ shown therein are given in Table 2. The extrapolation method used herein is invariably used to obtain hot spot stress (also know as geometric stress) in tubular joints, which considers the uneven stress distribution around the perimeter of the welded joint, and excludes effects related to configuration of the weld (and the local condition of the weld toe).

Commented [KT1]: Note change.

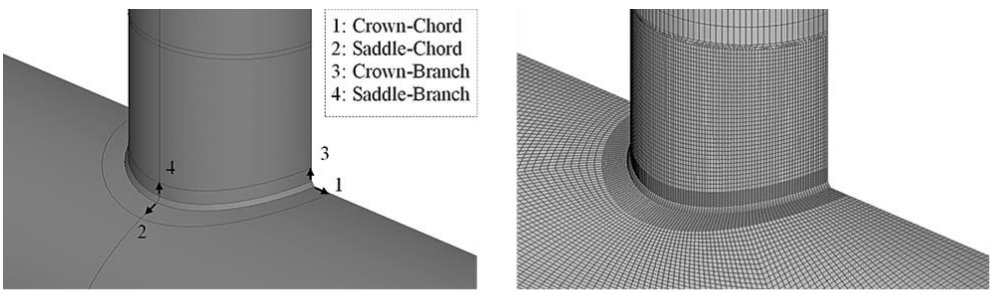

(a) Region partition (b) Mesh pattern

Fig. 5. Finite element modelling of welded joint *(two-column figure)*

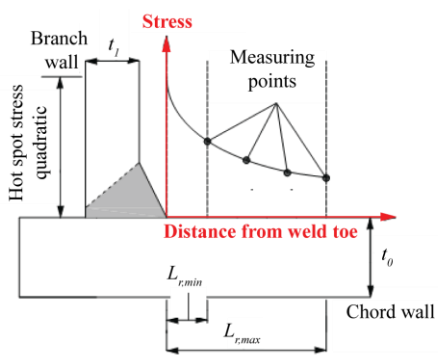

Fig. 6. Stress vs. distance from weld toe (adapted from [5]) (*one-column figure*)

Table 2. Boundaries of extrapolation region for CHS connections

	Chord		Branch	
Distance from weld toe	Saddle	Crown	Saddle	Crown
$L_{r,min}$ (1)	$0.4t_0$	$0.4t_0$	$0.4t_1$	$0.4t_1$
$L_{r,max}$ (2)	$0.09r_0$	$0.4(r_0t_0r_1t_1)^{0.25}$	$0.65(r_1t_1)^{0.5}$	$0.65(r_1t_1)^{0.5}$

Symbols: $L_{r,min}$ = distance from weld toe to end point of extrapolation zone; $L_{r,max}$ = distance from weld toe to starting point of extrapolation zone; r_0 = outer radius of chord member; and r_1 = inner radius of branch member.
(1) Minimum value for $L_{r,min}$ is 4 mm.
(2) Minimum value for $L_{r,max}$ is $L_{r,min} + 0.6t_1$.

To determine the SCFs in each FE connection model, a 50 kN axial compression force was incrementally applied to the branches. This was done so that the stresses around the welded joint could be monitored to ensure linear elastic behaviour. The branch nominal stress was then calculated by dividing the applied force by the branch cross-sectional area. The stresses perpendicular to the weld toe at different locations along the lines of interest (1, 2, 3 and 4, in Fig. 5a), within the extrapolation zones, were obtained from the FE model. Both the quadratic and linear extrapolation methods recommended by CIDECT DG8 [5] were evaluated. The former produced slightly larger (i.e. more conservative) hot spot stress values and was selected for the following analysis. Using the quadratic extrapolation method (described in Fig. 6 and Table 2), the hot spot stresses at the four critical locations (i.e. crown and saddle locations on both the branch and chord) were calculated. The SCFs at these locations were then calculated by dividing the hot spot stresses by the branch nominal stress. The SCFs obtained from the FE analyses are compared to the experimental data from HSE [21] in Table 3. As shown, reasonably good agreement was achieved, giving credence to the FE modelling approach.

Commented [KT2]: Note minor changes.

Table 3. Comparison of SCFs from experimental testing and finite element simulation

	SCFs							
	FE				FE / Experimental (2)			
Connection No.	Chord saddle	Chord crown	Branch saddle	Branch crown	Chord saddle	Chord crown	Branch saddle	Branch crown
1	11.5	- (1)	9	-	1.05	-	1.2	-
2	5.35	-	5.37	-	1.11	-	1.19	-
3	22.7	2.78	13.6	1.12	1.04	0.84	1.28	0.74
4	32.4	-	22	-	1.09	-	1.46	-

(1) Verifications were not performed at the locations where experimental data was unavailable.
(2) See Table 1 for experimental SCFs.

5.2 Preliminary finite element study on chord end distance effect

To evaluate the need for a comprehensive parametric study using the validated FE modelling approach, a preliminary FE study was performed. Eight "control models", with different β, and $e = 3d_0$ on both sides of the connection, served as the basis for the comparison. The value of $e = 3d_0$ was selected so that $\alpha > 12$ for all the control-model connections, to mitigate chord end-distance effects. From each of the control models, three new end-connection models were created with $e = d_0$, $0.5d_0$ and $0.1d_0$ on <u>one side</u> the connection (i.e. $e = 3d_0$ was maintained on the other side of the connection, as shown in Fig. 7). The lower bound of the end distance value, $e = 0.1d_0$, represents the shortest practical distance to an open chord end for a hollow section truss [12].

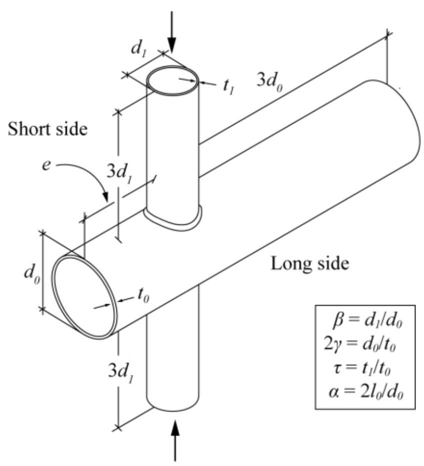

Fig. 7. Schematic diagram of FE models

The boundary conditions used for the control models were the same as those discussed in Section 5.1 of this paper. For the end connections, to simulate practical end connections with general chord fixity conditions, the end of the "short side" (see Fig. 7) was set free, while the end of the "long side" was pin-supported.

For the control models, the SCF formulae in CIDECT DG 8 [5] [i.e. Eqs. (4) to (13)] are applicable. Namely, $F_2 = 1$. All models included in the preliminary study are listed in Table 4, and typical, meshed FE models are shown in Fig. 8.

Table 4. Geometry of connection models for preliminary FE study (*one-column table*)

		Non-dimensional parameters [(1)]			
Chord (d_0×t_0) (mm)	Branch (d_1×t_1) (mm)	β	2γ	τ	e/d_0
300×15.0	135×12	0.45	20	0.8	3.0
300×15.0	135×12	0.45	20	0.8	1.0
300×15.0	135×12	0.45	20	0.8	0.5
300×15.0	135×12	0.45	20	0.8	0.1
300×8.6	135×6.9	0.45	35	0.8	3.0
300×8.6	135×6.9	0.45	35	0.8	1.0
300×8.6	135×6.9	0.45	35	0.8	0.5
300×8.6	135×6.9	0.45	35	0.8	0.1
300×6.0	135×4.8	0.45	50	0.8	3.0
300×6.0	135×4.8	0.45	50	0.8	1.0
300×6.0	135×4.8	0.45	50	0.8	0.5
300×6.0	135×4.8	0.45	50	0.8	0.1
300×4.6	135×3.7	0.45	65	0.8	3.0
300×4.6	135×3.7	0.45	65	0.8	1.0
300×4.6	135×3.7	0.45	65	0.8	0.5
300×4.6	135×3.7	0.45	65	0.8	0.1
300×15.0	180×12	0.60	20	0.8	3.0
300×15.0	180×12	0.60	20	0.8	1.0
300×15.0	180×12	0.60	20	0.8	0.5
300×15.0	180×12	0.60	20	0.8	0.1
300×8.6	180×6.9	0.60	35	0.8	3.0
300×8.6	180×6.9	0.60	35	0.8	1.0
300×8.6	180×6.9	0.60	35	0.8	0.5
300×8.6	180×6.9	0.60	35	0.8	0.1
300×6.0	180×4.8	0.60	50	0.8	3.0
300×6.0	180×4.8	0.60	50	0.8	1.0
300×6.0	180×4.8	0.60	50	0.8	0.5
300×6.0	180×4.8	0.60	50	0.8	0.1
300×4.6	180×3.7	0.60	65	0.8	3.0
300×4.6	180×3.7	0.60	65	0.8	1.0
300×4.6	180×3.7	0.60	65	0.8	0.5
300×4.6	180×3.7	0.60	65	0.8	0.1

[(1)] See Fig. 7 for non-dimensional parameter definitions.

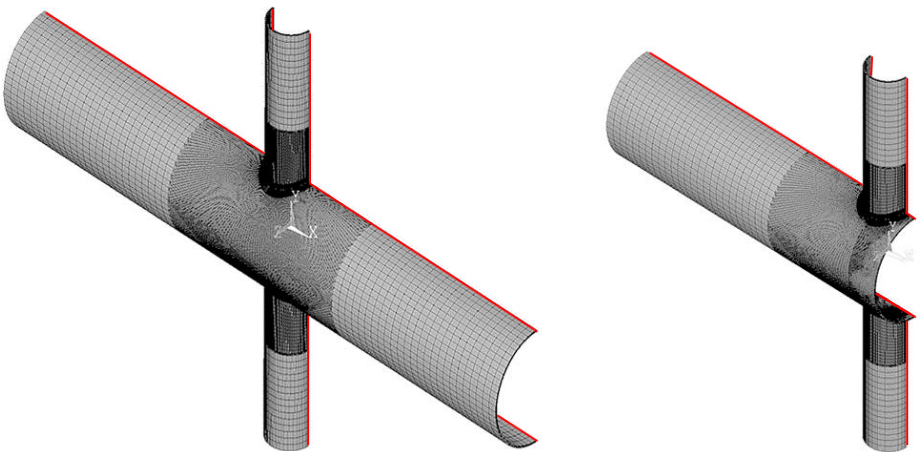

(a) Control model ($e/d_0 = 3$) (b) End connection model ($e/d_0 = 0.1$)

Fig. 8. Typical CHS-to-CHS axially loaded X-connection models (with different end distances)

For all models, the procedure described in Section 5.1 (i.e. the quadradic extrapolation technique) was used to calculate the hot spot stresses and, in turn, SCFs at the critical locations. For the control models, the SCFs were determined at the four critical locations (i.e. crown and saddle locations on the branch and chord). For the end connections, the SCFs were determined at:

a) the saddle location on both the branch and chord;
b) the crown location on both the branch and chord, on the "short side" of the connection (see Fig. 7); and
c) the crown location on both the branch and chord, on the "long side" of the connection (see Fig. 7).

According to the preliminary FE analysis, the SCFs at the two chord crown locations on the long and short sides of the end connections were nearly identical. (The same trend was observed in the full parametric study, discussed in Section 6). Conservatively, for each model, the larger these two SFCs was taken into consideration in the following analysis (and in Figs. 9 and 10). The same phenomenon was observed when comparing the branch crown SCFs on the long side and the short side, and the same approach (i.e. taking the larger value) was used.

Figs. 9 and 10 (on the following pages) show the ratios of SCFs in the end-connection models ($SCF_{end\ connection}$) to those in the control models ($SCF_{control\ model}$) – herein denoted as ψ – for all connections listed in Table 4. The ratio $\psi = SCF_{end\ connection}/\ SCF_{control\ model}$ is akin to the factor F_2 in Eq. (4).

The actual and extrapolated values of F_2 for the chord and branch saddle locations, using Eq. (13) [5] with the α value corresponding to the end distance of the "short side" (see Fig. 7), are shown superimposed atop the data in Figs. 9 and 10. The extrapolation region of the equation is noted therein (i.e. $\alpha \geq 4$, corresponding to $e/d_0 \geq 0.77$ and 0.70 for $\beta = 0.45$ and 0.60, respectively).

The following can be observed:

(1) According to Figs. 9 and 10, SCFs in end connections at all hot-spot locations can become significantly larger than those in the corresponding regular connections.

(2) The existing design charts in CIDECT DG8 [5] show that SCFs in general decrease with decreasing 2γ under branch axial loading. Similar trends can be observed in Figs. 9 and 10, which show that SCFs in some locations can be significantly larger when 2γ reaches 50, corresponding to d_0 = 300 mm and t_0 = 6 mm in the preliminary FE study models (Table 4).

(3) For the saddle locations, it is generally unsafe to extrapolate the existing "F_2" equation in CIDECT DG8 [5] [Eq. (13)] beyond its range of applicability. As shown in Figs. 9 and 10, extrapolation of the existing "F_2" formula leads to a reduction in predicted SCFs, in contrast to the trend(s) shown by the FE data.

(4) According to Figs. 9 and 10, the ψ-values are non-linearly related to e/d_0 decreases. The preliminary FE study results show that, in many cases, the highest SCFs occur when e/d_0 = 0.5 (not 0.1, as may have been expected).

(5) As the e/d_0-value approaches 3.0, the ψ-values in all cases converge to unity, where the chord length effect is negligible. This is consistent with the design rules in CIDECT DG8 [5].

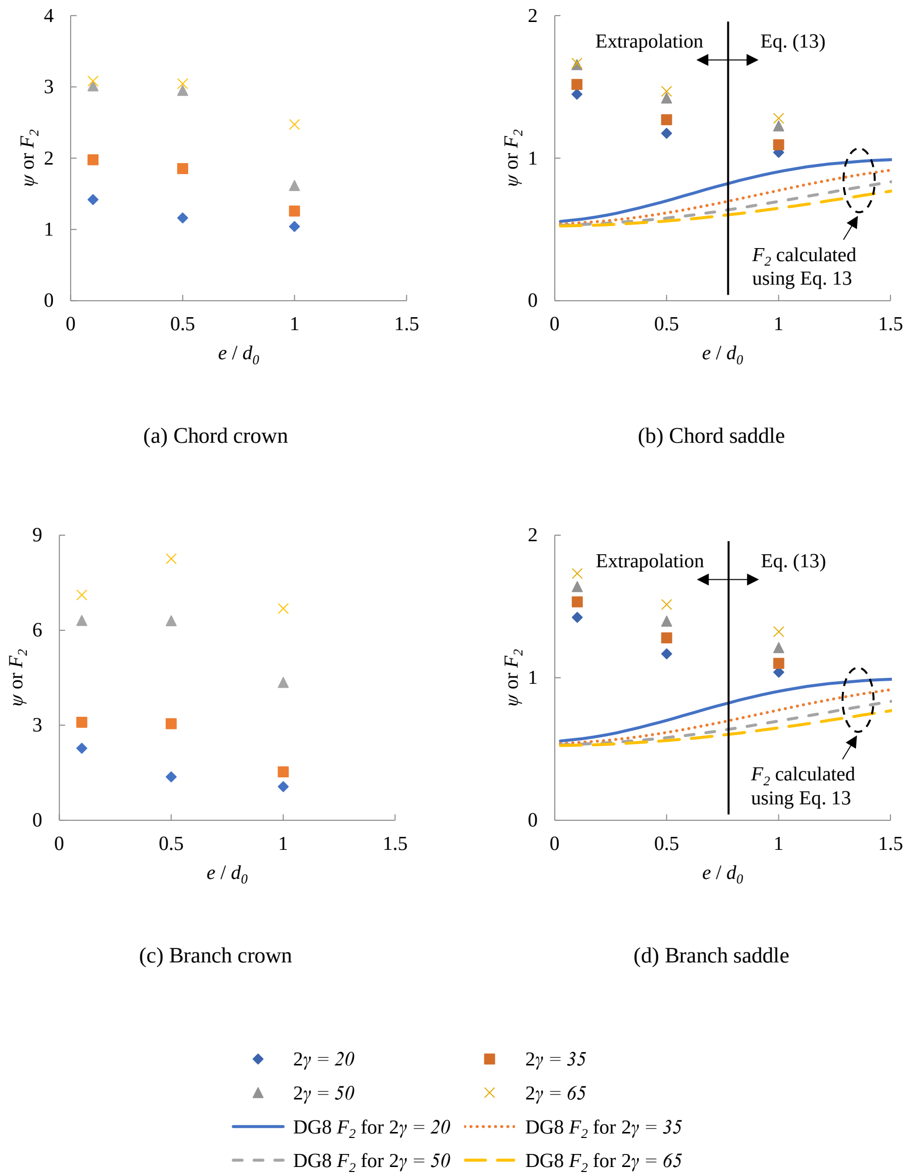

Fig. 9. SCFs for connection models in Table 4 with $\beta = 0.45$

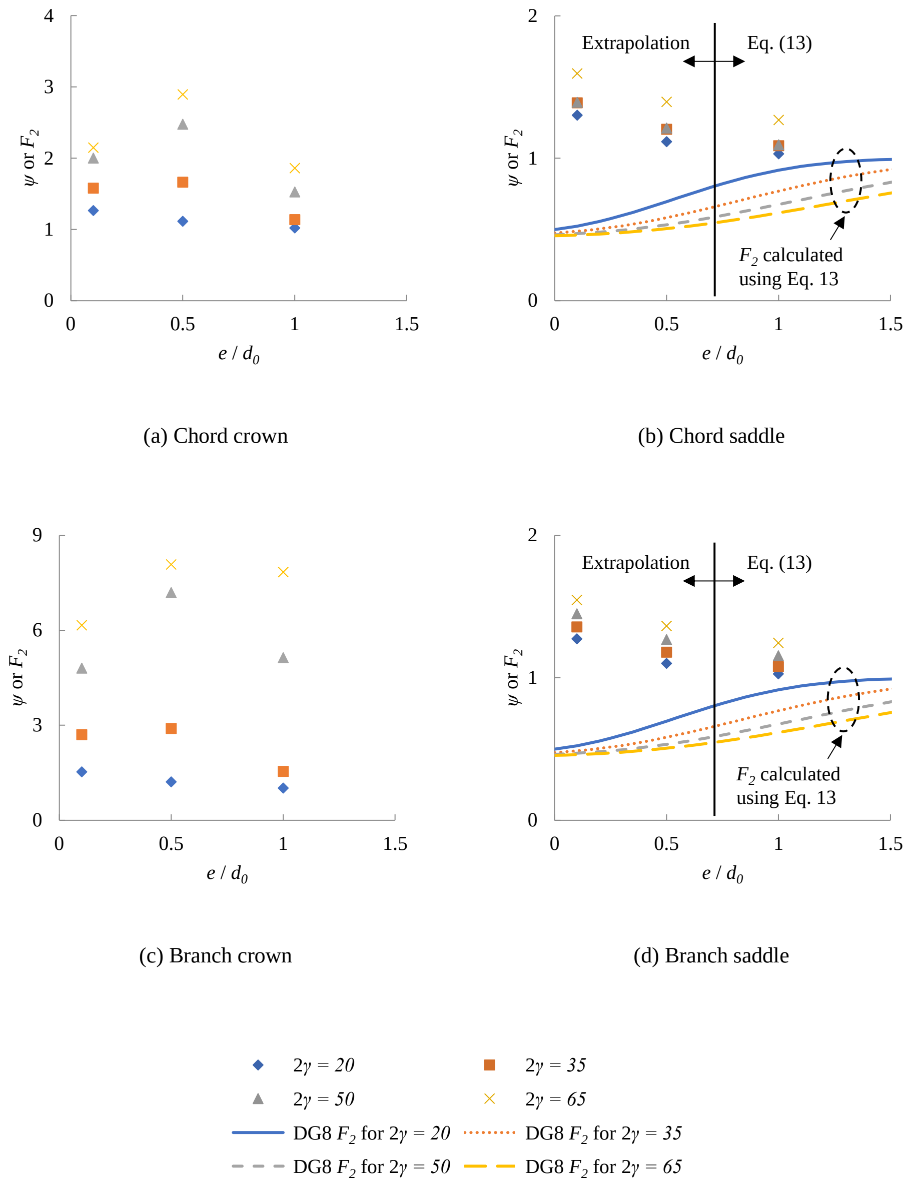

Fig. 10. SCFs for connection models in Table 4 with $\beta = 0.60$

6. Parametric study

As shown in the preliminary FE study described in Section 5.2, the chord end-distance effect can be significant on SCFs in CHS-to-CHS X-connections. Therefore, a subsequent comprehensive parametric FE study was deemed necessary to:

(1) explore the combined effects of a wider range of non-dimensional cross-sectional parameters (β, 2γ, and τ) and end distances (e); and

(2) develop new formulae for the prediction of SCFs in such connections.

A total of 240 FE models with chord members of a constant external diameter (d_0) of 300 mm were developed and analysed, with chord member thicknesses ranges from 2.4 to 15.0 mm. Other dimensions, including t_0, d_1 and t_1, and the end distance (e) were determined based on the selected non-dimensional parameters (β, 2γ and τ). Considering the limits of validity of the SCF equations for CHS-to-CHS X-connections in CIDECT DG8 [5] [Eqs. (3)-(13)], β, 2γ and τ were taken as:

- 2γ = 20, 35, 50 and 65;
- β = 0.30, 0.45, 0.60, and 0.75; and
- τ = 0.4, 0.6, 0.8, and 1.0.

The end distance (e) was varied between $0.1d_0$, $0.5d_0$, $1.0d_0$ and $3.0d_0$, with $3.0d_0$ representing a conservative upper limit beyond which end-distance effects could be safely ignored [12]. [Note that the corresponding α-values ($= 2l_0 / d_0$) for the e = $3.0d_0$ connections ranged from 12.6 to 13.5]. Figs. 11-13 show the representative results of ψ ($= SCF_{end\ connection}/ SCF_{control\ model}$) vs. e/d_0 at the four critical hot spot stress locations (as described, for the preliminary models, in Section 5.2). The following observations can be made:

(1) Nonlinear relationships between ψ and e/d_0 were observed for the chord and branch crown locations in Figs. 11 and 12.

(2) As shown in Fig. 11, for different values of e/d_0, as 2γ increases, ψ at the chord and branch crown locations increase significantly. (On the other hand, for the chord and branch saddle locations, the effect of 2γ on ψ follows a similar trend, but is less severe).

(3) Similarly, as shown in Fig. 12, for different values of e/d_0, as τ increases, ψ at the branch crown location increase significantly. (The effect of τ on ψ at the other hot-spot locations also follows a similar trend, but is less severe).

(4) As shown in Fig. 13, for different values of e/d_0, as β increases, the ψ-values all hot-spot locations decrease.

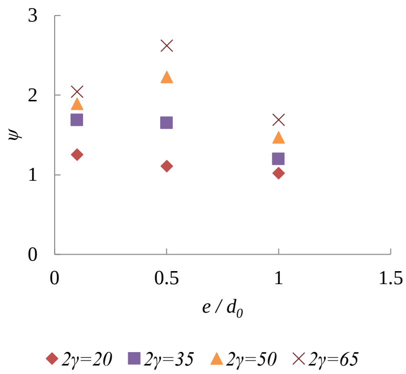

(a) Chord crown

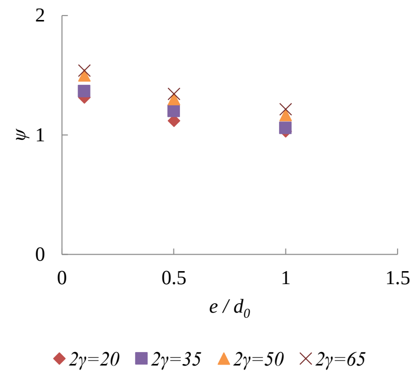

(b) Chord saddle

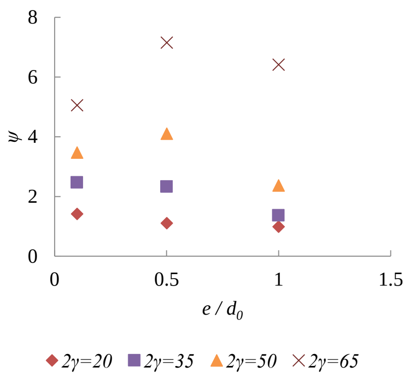

(c) Branch crown

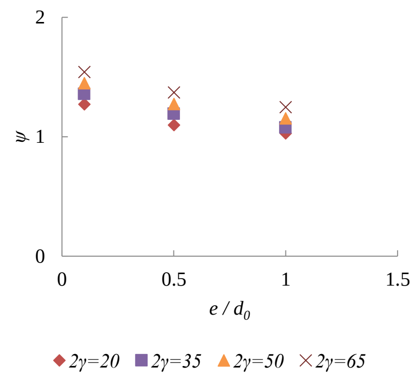

(d) Branch saddle

Fig. 11. Effects of e/d_0 and 2γ on SCFs in connections (β = 0.6 and τ = 0.6)

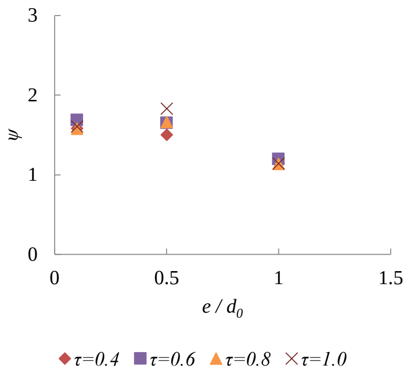

(a) Chord crown

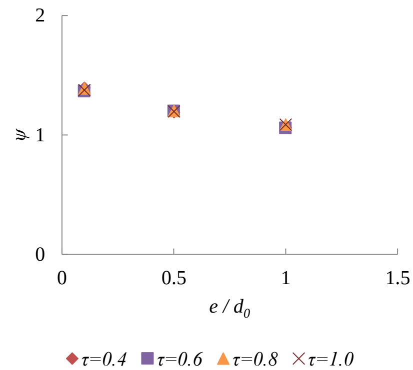

(b) Chord saddle

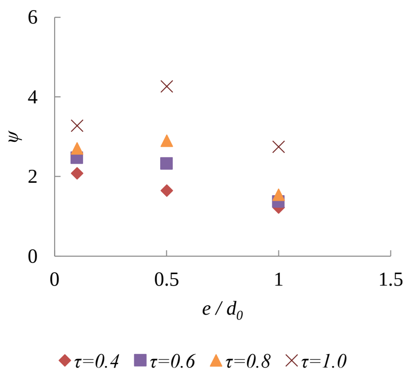

(c) Branch crown

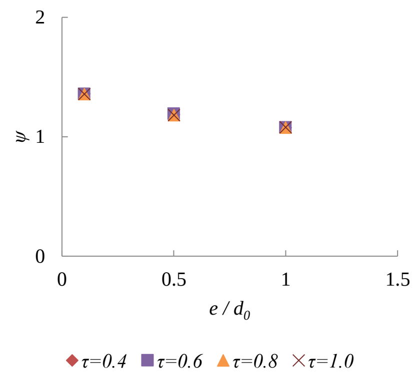

(d) Branch saddle

Fig. 12. Effects of e/d_0 and τ on SCFs in connections (β = 0.6 and 2γ = 35)

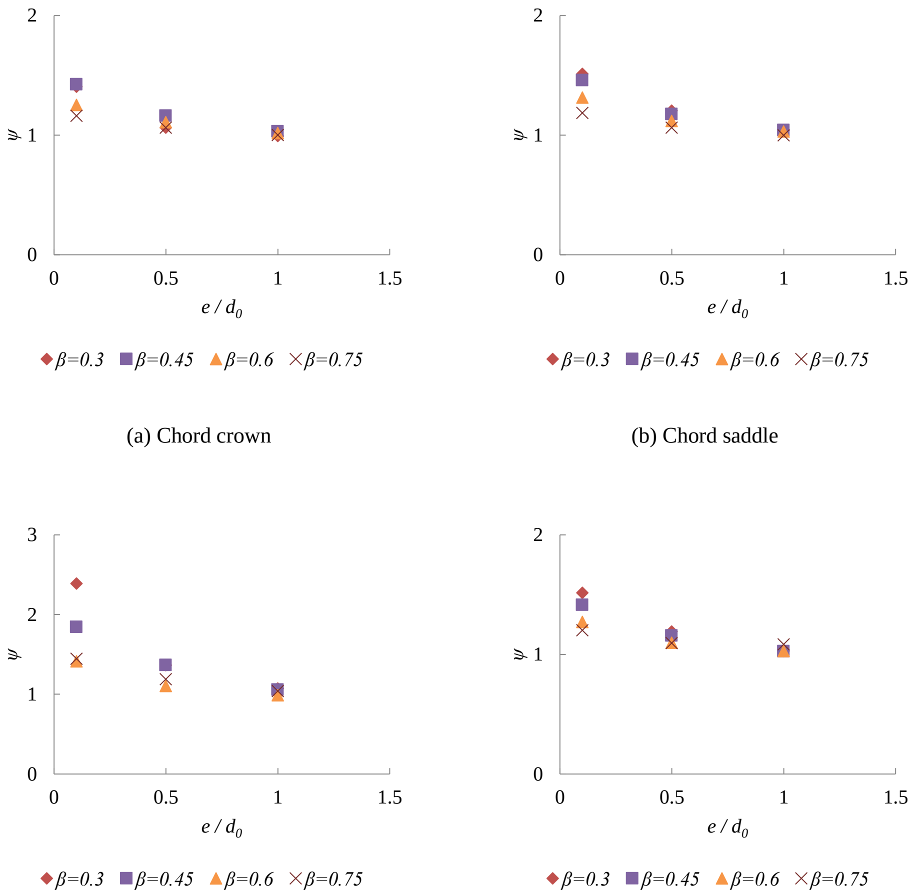

(a) Chord crown

(b) Chord saddle

(c) Branch crown

(d) Branch saddle

Fig. 13. Effects of e/d_0 and β on SCFs in connections (2γ = 20 and τ = 0.6)

7. Design Approach

According to the parametric study presented in Section 6, the existing SCF formulae in CIDECT DG8 [5] for regular CHS-to-CHS axially loaded X-connections, utilizing the F_2 factor [Eq. (13)], produce unsafe predictions when applied to CHS-to-CHS axially-loaded X-connections near an open chord end. A new design approach is hence proposed that aims to utilize the existing SCF formulae [Eqs. (8)-(11)] through the introduction of a correction coefficient (ψ) that correctly considers the chord end-distance effect, i.e.:

$$SCF_{end,i} = SCF_i \cdot \psi \qquad (14)$$

where $SCF_{end,i}$ = SCF at hot spot i in a CHS-to-CHS axially loaded X-connection near an open chord end; SCF_i = SCF at hot spot i in a CHS-to-CHS axially loaded X-connection [determined using Eqs. (8)-(11)]; and i = critical (hot spot) location (= chord saddle, chord crown, branch saddle and branch crown).

The correction coefficients (ψ) for all critical (hot spot) locations (A – E) for all 180 FE end connection models (i.e. 240 connection models less the 60 control models) analyzed in this study are listed in Table 5. These have been determined as previously described [i.e. by dividing the SCFs in the end-connection models by those in the control models ($\psi = SCF_{end\ connection} / SCF_{control\ model}$ in Table 5)].

Multiple nonlinear regression analyses were performed on the results in Table 5 to develop ψ-formulae that can be used to predict ψ based on the key non-dimensional variables identified in Section 6. The results of these analyses are summarized in Eqs. (15)-(17) below. As noted above Eq. (15), it was found that ψ at the branch and chord saddle points was similar in the same connections. Hence, a single equation is proposed to cover both locations [akin to how F_2 is currently used].

For the chord saddle and branch saddle:

$$\psi = 1.58 + 0.0053(2\gamma) + 0.80(e/d_0)(\beta)^2 - \beta^2 - 0.63(e/d_0) > 1 \qquad (15)$$

For the chord crown:

$$\begin{aligned}\psi &= 0.88(\beta) + 0.22\tau + 0.050(2\gamma) + 0.041(\beta)(2\gamma)(e/d_0) \\ &-0.033(2\gamma)(e/d_0)^2 - 0.069(2\gamma)(\beta)^2 > 1\end{aligned} \qquad (16)$$

For the branch crown:

$$\psi = 0.44(\tau)(\beta)(2\gamma) - \frac{0.65(\tau)(e/d_0)^3}{(\beta)} - 0.59(\tau)(2\gamma)(\beta)^3 > 1 \quad (17)$$

Eqs. (15)-(17) are valid within the ranges $0.3 \le \beta \le 0.75$, $20 \le 2\gamma \le 65$, and $0.4 \le \tau \le 1.0$. Table 6 provides key statistics on the accuracy of the equations relative to the 240 FE results. The comparisons show that the ratio of FE-to-predicted ψ is 0.99 or 1.00 for all four locations and – by virtue of having generally low coefficients of variation (COVs) – Eqs. (15) – (17) are acceptably accurate over the range of parameters considered.

Table 5. Correction factor ψ for CHS-to-CHS axially loaded X-connections near an open chord end

			e/d_0 = 1.0				e/d_0 = 0.5				e/d_0 = 0.1			
			Chord		Branch		Chord		Branch		Chord		Branch	
β	2γ	τ	Crown	Saddle	Crown	Saddle	Crown	Saddle	Crown	Saddle	Crown	Saddle	Crown	Saddle
0.3	20	0.4	0.97	1.01	1.03	1.04	1.12	1.17	1.31	1.18	1.54	1.53	1.84	1.50
0.3	20	0.6	0.99	1.04	1.07	1.03	1.06	1.20	1.36	1.19	1.41	1.51	2.39	1.51
0.3	20	0.8	1.01	1.05	0.79	1.05	1.03	1.21	1.35	1.23	1.33	1.56	2.96	1.61
0.3	20	1	1.02	1.05	0.74	1.05	1.17	1.22	2.36	1.24	1.51	1.58	4.63	1.60
0.3	35	0.4	1.19	1.08	1.34	1.11	1.66	1.36	1.87	1.30	2.23	1.69	2.52	1.60
0.3	35	0.6	1.23	1.13	1.40	1.12	1.60	1.36	1.99	1.34	2.10	1.67	2.67	1.63
0.3	35	0.8	1.24	1.13	1.36	1.10	1.61	1.36	2.49	1.32	2.08	1.66	3.10	1.60
0.3	35	1	1.24	1.13	2.21	1.03	1.62	1.36	4.85	1.33	2.13	1.65	5.74	1.59
0.3	50	0.4	1.45	1.22	1.69	1.20	2.22	1.46	2.37	1.46	2.69	1.75	3.01	1.69
0.3	50	0.6	1.52	1.24	1.80	1.22	2.31	1.47	2.56	1.46	2.51	1.75	3.24	1.72
0.3	50	0.8	1.56	1.24	2.04	1.21	2.31	1.48	3.24	1.45	2.59	1.75	3.72	1.70
0.3	50	1	1.58	1.24	3.63	1.16	2.39	1.48	4.94	1.43	2.62	1.74	5.81	1.68
0.3	65	0.6	1.85	1.32	2.55	1.32	3.19	1.56	3.62	1.51	3.35	1.78	4.36	1.78
0.3	65	0.8	1.91	1.34	3.47	1.30	3.01	1.58	5.19	1.53	3.18	1.79	5.69	1.77
0.3	65	1	1.94	1.34	5.94	1.28	3.06	1.58	7.63	1.47	3.15	1.78	7.77	1.70
0.45	20	0.4	1.03	1.04	1.07	1.03	1.15	1.18	1.35	1.14	1.40	1.48	1.87	1.43
0.45	20	0.6	1.03	1.04	1.05	1.02	1.16	1.18	1.36	1.15	1.42	1.46	1.84	1.41
0.45	20	0.8	1.04	1.04	1.06	1.04	1.16	1.17	1.36	1.17	1.42	1.45	2.27	1.42
0.45	20	1	1.03	1.03	1.06	1.03	1.16	1.17	2.24	1.16	1.40	1.44	3.51	1.41
0.45	35	0.4	1.18	1.12	1.16	1.10	1.54	1.32	1.68	1.32	1.93	1.60	2.22	1.51
0.45	35	0.6	1.23	1.12	1.11	1.11	1.79	1.31	1.73	1.34	1.90	1.57	1.98	1.58
0.45	35	0.8	1.26	1.09	1.53	1.10	1.85	1.27	3.05	1.28	1.98	1.52	3.09	1.53
0.45	35	1	1.26	1.06	2.65	1.11	1.98	1.23	4.19	1.26	2.01	1.46	4.72	1.49
0.45	50	0.4	1.45	1.21	1.96	1.19	2.49	1.42	3.31	1.38	2.76	1.68	3.47	1.61
0.45	50	0.6	1.56	1.23	2.49	1.20	2.66	1.43	4.63	1.39	2.87	1.68	4.90	1.63
0.45	50	0.8	1.62	1.23	4.35	1.21	2.95	1.42	6.30	1.40	3.01	1.66	6.31	1.64
0.45	50	1	1.74	1.22	6.59	1.18	2.75	1.41	6.78	1.37	2.89	1.64	6.83	1.60
0.45	65	0.6	2.23	1.18	4.76	1.31	3.05	1.37	6.04	1.50	3.10	1.56	6.47	1.72
0.45	65	0.8	2.47	1.28	6.68	1.32	3.04	1.47	8.26	1.51	3.08	1.67	7.11	1.73
0.45	65	1	2.63	1.25	8.26	1.21	2.90	1.43	9.06	1.39	2.97	1.64	8.75	1.59
0.6	20	0.4	1.01	1.00	0.99	1.02	1.09	1.09	1.17	1.09	1.22	1.30	1.51	1.27
0.6	20	0.6	1.02	1.03	0.99	1.03	1.11	1.12	1.10	1.10	1.25	1.31	1.41	1.27
0.6	20	0.8	1.02	1.03	1.01	1.03	1.11	1.12	1.21	1.10	1.26	1.30	1.53	1.27
0.6	20	1	1.02	1.03	1.06	1.03	1.11	1.11	1.35	1.10	1.25	1.29	1.84	1.27
0.6	35	0.4	1.14	1.06	1.22	1.07	1.50	1.19	1.64	1.18	1.58	1.39	2.08	1.36
0.6	35	0.6	1.20	1.06	1.36	1.08	1.65	1.20	2.32	1.19	1.69	1.36	2.46	1.36
0.6	35	0.8	1.14	1.09	1.54	1.08	1.66	1.20	2.90	1.18	1.58	1.39	2.70	1.36
0.6	35	1	1.14	1.09	2.75	1.08	1.83	1.20	4.26	1.18	1.61	1.38	3.28	1.36
0.6	50	0.4	1.38	1.09	1.47	1.15	2.15	1.23	2.14	1.28	1.72	1.42	2.44	1.45
0.6	50	0.6	1.47	1.17	2.36	1.15	2.23	1.30	4.10	1.27	1.89	1.50	3.46	1.45
0.6	50	0.8	1.53	1.09	5.13	1.15	2.48	1.21	7.19	1.27	2.00	1.39	4.80	1.45
0.6	50	1	1.65	1.17	7.80	1.15	2.72	1.29	9.05	1.27	2.05	1.48	6.36	1.45

Table 5 (cont'd). Correction factor ψ for CHS-to-CHS axially loaded X-connections near an open chord end

			e/d_0 = 1.0				e/d_0 = 0.5				e/d_0 = 0.1			
			Chord		Branch		Chord		Branch		Chord		Branch	
β	2γ	τ	Crown	Saddle	Crown	Saddle	Crown	Saddle	Crown	Saddle	Crown	Saddle	Crown	Saddle
0.6	65	0.6	1.69	1.22	6.41	1.25	2.62	1.34	7.14	1.37	2.04	1.54	5.05	1.54
0.6	65	0.8	1.86	1.27	7.84	1.24	2.89	1.40	8.08	1.36	2.15	1.59	6.16	1.55
0.6	65	1	2.08	1.26	8.94	1.24	3.15	1.38	9.87	1.36	2.21	1.58	8.04	1.55
0.75	20	0.4	1.00	1.01	1.04	1.02	1.04	1.06	1.17	1.06	1.11	1.18	1.39	1.15
0.75	20	0.6	1.00	1.00	1.04	1.08	1.06	1.06	1.19	1.09	1.16	1.19	1.45	1.20
0.75	20	0.8	1.10	0.98	1.04	1.07	1.06	1.05	1.16	1.05	1.14	1.16	1.35	1.14
0.75	20	1	1.00	0.99	1.01	1.02	1.06	1.02	1.12	1.05	1.14	1.15	1.29	1.16
0.75	35	0.4	1.09	1.00	0.73	1.05	1.22	1.07	1.08	1.11	1.27	1.18	1.27	1.20
0.75	35	0.6	1.13	1.05	1.11	1.04	1.29	1.12	1.35	1.10	1.37	1.22	1.60	1.19
0.75	35	0.8	1.14	1.05	1.29	1.04	1.36	1.11	1.61	1.09	1.42	1.21	1.94	1.18
0.75	35	1	1.00	1.05	1.39	1.04	1.36	1.10	2.32	1.09	1.45	1.20	2.30	1.18
0.75	50	0.4	1.26	1.11	1.44	1.10	1.56	1.19	1.77	1.18	1.57	1.31	2.09	1.26
0.75	50	0.6	1.32	1.10	1.79	1.09	1.73	1.17	2.21	1.16	1.58	1.29	2.62	1.24
0.75	50	0.8	1.30	1.10	1.88	1.13	1.85	1.16	2.97	1.19	1.54	1.27	2.80	1.28
0.75	50	1	1.33	1.09	3.07	1.09	2.09	1.15	4.86	1.14	1.59	1.26	3.55	1.23
0.75	65	0.6	1.48	1.13	2.90	1.16	1.74	1.20	4.21	1.22	1.82	1.32	3.40	1.31
0.75	65	0.8	1.52	1.16	3.71	1.15	1.93	1.22	5.15	1.21	1.77	1.34	3.87	1.30
0.75	65	1	1.54	1.15	4.38	1.16	2.10	1.21	5.96	1.21	1.76	1.33	4.53	1.29

Table 6. Mean values and COVs of FE-to-predicted ψ based on 240 FE results

Location	Equation No.	Mean	COV
Chord Saddle	(15)	1.00	0.03
Chord Crown	(16)	0.99	0.08
Branch Saddle	(15)	1.00	0.03
Branch Crown	(17)	0.99	0.21

8. Conclusions

In this paper, 240 3D FE models were developed to analyse axially loaded CHS-to-CHS X-connections near an open chord end. Models were verified using previously reported experimental results, and a parametric study was conducted to explore the effects of end distance (e/d_0) and other key non-dimensional parameters (β, 2γ and τ) on so called "chord end-distance effects" on SCFs. Key findings are as follows:

1. SCFs at all hot-spot location vary non-linearly as a function of e/d_0 and can become significantly larger than those in the corresponding regular connections.

2. For the saddle locations, it is unsafe to extrapolate the existing "F_2" equation in CIDECT DG8 [5] [Eq. (13)] beyond its range of applicability. This will lead to a reduction in predicted SCFs, in contrast to (1).
3. For different values of e/d_0:
    a. as 2γ increases, SCFs at chord and branch crown locations increase significantly. (For the chord and branch saddle locations, the effect of 2γ on SCFs follows a similar trend, but is less severe).
    b. as τ increases, SCFs at the branch crown location increase significantly. (For the other hot-spot locations, the effect of 2γ on SCFs follows a similar trend, but is less severe).
    c. as β increases, SCFs at all hot-spot locations decrease.

Based on these key findings, parametric equations were developed to estimate SCF correction coefficients (ψ) to relate SCFs in axially loaded CHS-to-CHS end connections those in regular connections at the critical (hot spot) stress locations. These ψ-formulae are intended to be used in conjunction with existing SCF equations for so-called regular connections from CIDECT DG8 [5], by multiplying the result of Eqs. (8) to (11) by ψ to determine the SCF. The SCF correction coefficients (ψ) formulae are valid within the ranges $0.3 \leq \beta \leq 0.75$, $20 \leq 2\gamma \leq 65$, and $0.4 \leq \tau \leq 1.0$. The fatigue life of CHS-to-CHS axially-loaded X-connections near an open chord end can then be determined by using S-N curves for standard connections. It is deemed necessary to expand this research to include other connection types and loading conditions.

Acknowledgements

The authors would like to express their appreciation to the Natural Sciences and Engineering Research Council of Canada (NSERC) for providing the financial support for this research.

Nomenclature

E	Young's modulus
F_2	reduction factor to account for "end effects" in CIDECT Design Guide 8
$L_{r,max}$	distance from weld toe to end point of extrapolation zone
$L_{r,min}$	distance from weld toe to starting point of extrapolation zone
$SCF_{b\_crown,ax}$	branch SCF at the crown point
$SCF_{b\_saddle,ax}$	branch SCF at the saddle point
$SCF_{ch\_crown,ax}$	chord SCF at the crown point

$SCF_{ch\_saddle,ax}$ chord SCF at the saddle point

$SCF_{end\ connection}$ SCF in end-connection model

$SCF_{control\ model}$ SCF in control model (connection with sufficient chord continuity)

X_{1-4} SCF parameter for CHS-to-CHS X-connections

b_0 RHS chord width

b_1 RHS branch width

b_p branch plate width

d_0 CHS chord diameter

d_1 CHS branch diameter

e end distance = distance from the heel/toe of the closest branch to the chord end

e_{min} minimum required end distance

l_0 chord length

r_1 inner radius of branch member

r_0 outer radius of chord member

t_0 chord wall thickness

t_1 branch wall thickness

α chord length parameter (= $2l_0/d_0$)

β branch-to-chord diameter ratio (= d_1/d_0); branch-to-chord width ratio (= b_1/b_0)

γ half chord diameter-to-thickness ratio (= $d_0/2t_0$); half chord width-to-thickness ratio (= $b_0/2t_0$)

τ branch-to-chord thickness ratio (= t_1/t_0)

θ acute angle between the branch and chord (in degrees)

ψ reduction factor for end connection

References

[1] J.A. Packer, J.E. Henderson, Hollow Structural Section Connections and Trusses – a Design Guide, 2nd ed. Canadian Institute of Steel Construction, Toronto, Canada, 1997.

[2] J. Wardenier, Y. Kurobane, J.A. Packer, A. van der Vegte, X.L. Zhao, Design Guide for Circular Hollow Section (CHS) Joints under Predominantly Static Loading, CIDECT Design Guide No. 1, 2nd ed. CIDECT, Geneva, Switzerland, 2008.

[3] J.A. Packer, J. Wardenier, X.L. Zhao, G.J. van der Vegte, Y. Kurobane, Design Guide for Rectangular Hollow Section (RHS) Joints under Predominantly Static Loading, CIDECT Design Guide No. 3, 2nd ed. CIDECT, Geneva, Switzerland, 2009.

[4] ISO (International Organization for Standardization), ISO 14346:2013, Static Design Procedure for Welded Hollow Section Joints – Recommendations, Geneva, Switzerland, 2013.

[5] X.L. Zhao, S. Herion, J.A. Packer, R.S. Puthli, G. Sedlacek, J. Wardenier, K. Weynand, A.M. van Wingerde, N.F. Yeomans, Design Guide for Circular and Rectangular Hollow Section Welded Joints under Fatigue Loading, CIDECT Design Guide No. 8, CIDECT and Verlag TÜV Rheinland GmbH, Köln, Germany, 2001.

[6] ISO (International Organization for Standardization), ISO 14347:2008, Fatigue – Design Procedure for Welded Hollow-Section Joints – Recommendations, Geneva, Switzerland, 2008.

[7] AISC (American Institute of Steel Construction), ANSI/AISC 360-16, Specification for Structural Steel Buildings. Chicago, IL, USA, 2016.

[8] J.A. Packer, D.R. Sherman, M. Lecce, Design Guide No. 24, Hollow Structural Section Connections. American Institute of Steel Construction, Chicago, IL, USA, 2010.

[9] CEN (European Committee for Standardization), EN 1993-1-8:2010, Eurocode 3: Design of steel structures – Part 1–8: Design of Joints, Brussels, Belgium, 2010.

[10] ISO (International Organization for Standardization), ISO 14347:2008, Fatigue – Design Procedure for Welded Hollow-Section Joints – Recommendations, Geneva, Switzerland, 2008.

[11] Y.J. Fan, J.A. Packer, RHS-to-RHS axially loaded X-connections near an open chord end. Canadian Journal of Civil Engineering 44 (2017) 881-892.

[12] X.D. Bu, J.A. Packer. Chord end distance effect on RHS connections. Journal of Constructional Steel Research, 168 (2020) 105992.

[13] CEN (European Committee for Standardization), Eurocode 3: Design of steel structures – Part 1–8: Design of joints. prEN 1993-1-8:2018, Brussels, Belgium, 2018.

[14] A.P. Voth, J.A. Packer, Branch plate-to-circular hollow section connections. II: X-type parametric numerical study and design. Journal of Structural Engineering, American Society of Civil Engineers, 138(8) (2012) 1007–1018.

[15] A.P. Voth, J.A. Packer, Numerical study and design of T-type branch plate-to-circular hollow section connections. Engineering Structures 41 (2012) 477–489.

[16] G.J. van der Vegte, Y. Makino, Further research on chord length and boundary conditions of CHS T- and X-joints. Advanced Steel Construction 6(3) (2010) 879-890.

[17] G.J. van der Vegte, Y. Makino, Ultimate strength formulation for axially loaded CHS uniplanar T-joints, International Journal of Offshore and Polar Engineering (2006) 16(4) 305-312.

[18] K. Tousignant, Effect of chord length and boundary conditions on welds in CHS X-joints. Proceedings of the 17th International Symposium on Tubular Structures, Singapore (2019) 63-70.

[19] S. Danashvar, M. Sun, K. Tousignant, Stress concentration factors for RHS-to-RHS X-connections near an open chord end. Journal of Constructional Steel Research (2020) (submitted).

[20] M. Efthymiou, S. Durkin, Stress concentration in T/Y and gap/overlap K-joints, Proceedings of the 4th International Conference on Behaviour of Offshore Structures, Amsterdam, The Netherlands (1985) 429–440.

[21] HSE (Health and Safety Executive), OTH 354: stress concentration factors for simple tubular joints-assessment of existing and development of new parametric formulae, prepared by Lloyd's Register of Shipping. Norwich, UK, 1997.

[22] Swanson Analysis Systems, ANSYS ver. 14.0. Houston, TX, USA, 2011.

[23] B. Cheng, Q. Qian, X.L. Zhao, Numerical investigation on stress concentration factors of square bird-beak SHS T-joints subject to axial forces. Thin-Walled Structures 94 (2015) 435-445.

[24] L.W. Tong, G.W. Xu, Y.Q. Liu, D.Q. Yan, X.L. Zhao, Finite element analysis and formulae for stress concentration factors of diamond bird-beak SHS T-joints. Thin-Walled Structures 86 (2015) 108-120.

[25] L.W. Tong, G.W. Xu, D.L. Yang, F.R. Mashiri, X.L. Zhao, Stress concentration factors in CHS-CFSHS T-joints: experiments, FE analysis and formulae. Engineering Structures 151 (2017) 406-421.

[26] R. Feng, B. Young, Stress concentration factors of cold-formed stainless steel tubular X-joints. Journal of Constructional Steel Research 91 (2013) 26-41.

[27] K. Tousignant, J.A. Packer Weld effective lengths for rectangular HSS overlapped K-connections. Engineering Journal, American Institute of Steel Construction, 52 (2015) 259-282.

[28] M. Yaghoubshahi, M. Sun, K. Tousignant, Design of fillet welds in RHS-to-RHS moment T-connections under branch in-plane bending. Journal of Constructional Steel Research 159 (2019) 122-133.

[29] K. Tousignant, J.A. Packer, Fillet weld effective lengths in CHS X-connections. I: Experimentation. Journal of Constructional Steel Research 128 (2017) 420-431.

[30] K. Tousignant, J.A. Packer, Numerical investigation of fillet welds in HSS-to-rigid end-plate connections. Journal of Structural Engineering, ASCE 143(12) (2017) 04017165:1-04017165-16.

[31] K. Tousignant, J.A. Packer, Fillet weld effective lengths in CHS X-connections. II: Finite element modelling, parametric study and design. Journal of Constructional Steel Research 141 (2018) 77-90.

[32] K. Tousignant, J.A. Packer, Weld effective lengths for round HSS cross-connections under branch axial loading. Engineering Journal, AISC 56(3) (2019) 173-186.

[33] K. Tousignant, J.A. Packer, Fillet welds around circular hollow sections. Welding in the World, IIW 63 (2019) 421-433.

[34] H. Ahmadi, A. Ziaei Nejad, Local joint flexibility of two-planar tubular DK-joints in OWTs subjected to axial loading: parametric study of geometrical effects and design formulation. Ocean Engineering 136(5) (2017) 1-10.

[35] H. Ahmadi, A. Ziaei Nejad, A study on the local joint flexibility (LJF) of two-planar tubular DK-joints in jacket structures under in-plane bending loads. Applied Ocean Research 64(3) (2017) 1-14.

[36] H. Ahmadi, A. Ziaei Nejad, Geometrical effects on the local joint flexibility of two-planar tubular DK-joints in jacket substructure of offshore wind turbines under OPB loading. Thin-Walled Structures 114(5) (2017) 122-133.

[37] H. Ahmadi, A. Ziaei Nejad, Stress concentration factors in uniplanar tubular KT-joints of jacket structures subjected to in-plane bending loads. International Journal of Maritime Technology 5(2) (2016) 27-39.

[38] S. Daneshvar, M. Sun, K. Karimi, Galvanized RHS X-connections. I: effects of vent and drain holes on SCFs. Journal of Constructional Steel Research (2020) 105854.

[39] S. Daneshvar, M. Sun, Stress concentration factors of RHS T-connections with galvanizing holes under in-plane bending. Journal of Constructional Steel Research 169 (2020) 106039.